International Journal of Heat and Mass Transfer 227 (2024) 125518

Contents lists available at ScienceDirect

International Journal of Heat and Mass Transfer

journal homepage: www.elsevier.com/locate/ijhmt

Utilizing Ragone framework for optimized phase change material-based heat sink design in electronic cooling applications

Ayushman Singh, Srikanth Rangarajan *, Bahgat Sammakia

Department of Mechanical Engineering, State University of New York at Binghamton, Binghamton, NY, USA

ARTICLE INFO

Keywords:
Phase change materials
Thermal energy storage
Porous foam

ABSTRACT

This study explores the latent thermal energy storage potential of an organic phase change material with porous copper foam and its applicability in electronic cooling under varying heat load conditions. The organic phase change material, n-eicosane, is known for its inherently low thermal conductivity of 0.15 W/mK, rendering it vulnerable during power spikes despite its abundant latent heat energy for phase transition from solid to liquid. Porous copper foams are often integrated into n-eicosane to enhance the composite's thermal conductivity. However, the volume fraction of the phase change material in the porous foam that optimally improves the thermal performance can be dependent on the boundary condition, the cut-off temperature, and the thickness. A finite difference numerical model was developed and utilized to ascertain the energy consumption for the composite of n-eicosane with two kinds of porous copper foam with varying porosity under different heat rates, cut-off temperatures, and thickness. In addition, the results are compared with a metallic phase change material (gallium), a material chosen with a similar melting point but significantly high thermal conductivity and volumetric latent heat. For validation of the numerical model and to experimentally verify the effect of boundary condition (heat rate), experimental investigation was performed for n-eicosane and high porosity copper foam composite at varying heat rates to observe its melting and solidification behaviors during continuous operation until a cut-off temperature of 70 °C is reached. Experiments reveal that heat rate influences the amount of latent energy storage capability until a cutoff temperature is reached. For broad comparison, the numerical model was used to obtain the accessed energy and power density and generate thermal Ragone plots to compare and characterize pure gallium and n-eicosane - porous foam composite with varying volume fractions, cutoff temperature, and thickness under volumetric and gravimetric constraints. Overall, the proposed framework in the form of thermal Ragone plots effectively delineates the optimal points for various combinations of heat rate, cut-off point, and aspect ratio, affirming its utility for comprehensive design guidelines for PCM-based composites for electronic cooling applications

1. Introduction

Thermal energy storage (TES) using the phase change materials' latent energy has shown benefits in peak shaving and load shifting in buildings, storing heat generated while operating lithium-ion batteries, and mitigating the temperature rise in electronic devices [1–5]. A phase change material (PCM) changes phase from solid to liquid by utilizing its latent heat of fusion and maintaining a temperature near the melting point or phase transition temperature. In electronic devices, the temperature rise beyond a maximum allowable limit or cut-off point can be mitigated by utilizing PCM's latent thermal energy storage. However, the PCM must be resolidified to take another melting process in the next cycle or power surge. The maximum allowable temperature limit varies with the applications, though mainly in electronic cooling; the threshold temperature for safe operation of the devices is 70 - 80 °C [6].

Moreover, an additional threshold on the temperature at the outside surface of the device can also be critical for portable or handheld devices. The user's thermal comfort dictates the threshold on the outer surface and is typically considered to be ~ 45 °C [7]. Categories of PCMs in thermal energy storage for electronic cooling applications include alkanes, salt hydrates, metallic, and low melting point eutectic alloys [1,4,8,9]. Organic PCMs, like alkanes, have high latent heat and are available in various phase transition temperatures. Hence, they can be a good candidate when choosing the PCM. The major disadvantage,

* Corresponding author.
E-mail address: srangar@binghamton.edu (S. Rangarajan).

https://doi.org/10.1016/j.ijheatmasstransfer.2024.125518
Received 29 November 2023; Received in revised form 2 March 2024; Accepted 28 March 2024
Available online 17 April 2024

however, is the low thermal conductivity of the organic PCMs, which makes it challenging to consume the latent energy available while operating below a maximum cut-off temperature for device safety. The low thermal conductivity, therefore, leads to low power density (the rate at which the available energy is accessed) for the high energy density (available energy) in the PCM [10]. Thermal conductivity-enhancing filler materials are often used along with the organic PCMs to enhance thermal conduction and increase the power density. The most commonly used techniques are the addition of fins, foams, and honeycomb structures of high thermal conductivity materials like aluminum or copper [11–14].

In recent years, metal foams have been extensively used as thermal conductivity fillers because of their low mass density and high area density for heat transfer [2,4,15–17]. The area density can be further enhanced by increasing the pore density of the foam used [18,19]. Yang et al. [4] used porous metal foam with Field's metal (a low melting point eutectic alloy) for thermal buffering of pulsed heat loads. The experiments were coupled with an FEM model to determine the cooling capacity figure of merit, effective thermal conductivity, energy density, and buffering time constant. The copper foam and Field's metal composite cooling capacity figure of merit was around 1.6 and 9 times the theoretical values of the aluminum-paraffin composite and pure paraffin wax, respectively. The authors also developed the design guidelines for thermal buffer devices for thermal management during pulsed heating conditions. Adding the high porosity open-celled copper foam can enhance the effective thermal conductivity of the composite with PCM by almost thirteen times compared to the pure PCM with just an addition of around 3 % volume/volume of copper foam [9]. The addition of graphene coating to the metal foam has also shown improvement in the heat conduction to the PCM. In work by Hussain et al. [20], the thermal management of a lithium-ion battery was demonstrated with the graphene-coated Nickel foam. They reported an effective thermal conductivity enhancement of around 23 times with the graphene-coated Nickel foam compared to pure paraffin. Fan et al. [21] also conducted experiment tests on a thermal energy storage system using a liquid metal Pb-Sn-In-Bi alloy and organic Octadecanol as PCM with roughly the same melting temperature. In their analysis, the liquid metal PCM performed better than the organic PCM due to high thermal conductivity in the liquid metal for comparable volumetric latent heat. However, the study was conducted only for a fixed volume of both the PCMs, whereas, for the applications involving the TES system to be mobile, fixed mass as a constraint can also be critical. Rehman and Ali [22] investigated the thermal performance of paraffin wax integrated with copper foam with 95 % and 97 % porosity at three power levels. They reported that 95 % porosity foam always performed the best by lowering the maximum temperature at the heated side [22–25].

Researchers perform many numerical investigations to model the composite of PCM and porous foam composite. Meng et al. [17] numerically investigated the melting time and transient temperature response while varying the porosity and pore density of the copper foam impregnated with paraffin. They found that by increasing the porosity from 88 % to 98 %, melting time increased, whereas, at a fixed porosity of 94 %, melting time reduced with the increasing pore density. Also, the temperature response rate was higher for 88 % porosity foam; however, the numerical simulations were done for a constant temperature boundary condition. In the context of electronic cooling, the importance lies in the energy storage until a cut-off temperature is reached; therefore, the thermal responsiveness of the PCM-based composite is more critical with heat flux boundary conditions. Sundaram and Li [19] used a finite element model to study the effect of pore size and porosity of aluminum foam with paraffin wax as PCM. They found that the convection in the molten PCM did not significantly affect the transient temperature when the results were compared with experiments due to the low velocity of the molten PCM. They also observed the effect of porosity at low and high heat generation rates. The effect of porosity was indistinguishable at low heat generation, whereas the thermal performance was better for high porosity at high heat generation rate. This effect is counter-intuitive as a higher heat generation rate would demand more metal volume to enhance the thermal conductivity and responsiveness. Also, the heat rate at which adding more metal would improve thermal performance is unknown. Therefore, the thermal performance needs to be quantified at several heat rates. Two techniques are commonly used to model the phase change in the PCM integrated with the foam: the thermal equilibrium model and the thermal non-equilibrium model. In the thermal equilibrium, a single energy equation is solved for the composite's effective medium with effective thermophysical properties, assuming zero temperature jump at the contact of foam ligaments and PCM. In the case of the thermal non-equilibrium model, energy equations are solved separately for the individual zones of porous foam and PCM [23,24]. The thermal non-equilibrium model with the buoyancy-driven fluid flow of PCM has been reported as more accurate in capturing physics [15,23]. However, the simplified thermal equilibrium model has the merit of reducing the computation time and cost.

In literature, the time to reach a set point or cut-off temperature or the temperature at the end of the heating time is often considered as a performance metric to quantify the thermal performance of the PCM or PCM-based composites [22,25–27]. These performance metrics can be correlated to the actual latent energy accessed in the PCM; however, the latent energy accessed in the PCM can be different at varying rates of heat supply, cut-off temperature, and geometry (aspect ratio/thickness). Many data points are needed with these variables to obtain the trend for various materials and volume fractions of foam. This development can be expensive with experimentation or high-fidelity numerical simulations; therefore, a simplified numerical model can be a helpful tool for comparing different cases.

In recent years, a cooling capacity figure of merit (FoM) has been proposed to design a PCM-based heat sink. However, FoM mainly derives from the heat sink's effective thermal conductivity and latent heat [5,28–30]. The FoM, therefore, can give an estimate on the balance of the thermal conduction and the heat storage capacity but cannot be beneficial if the operating conditions, geometry, and cut-off conditions are changed as the FoM is a combination of the material properties. As the boundary condition, for instance, the rate at which the heat is supplied to the heat sink is varied, the responsiveness of a PCM-based heat sink can be changed. In another work, a new figure of merit is proposed that modifies the conventional FoM by including a performance factor for the dependence of the geometry on the thermal performance [31]. However, the literature data does not present a detailed analysis of the effect of thermal boundary, cut-off temperature, and aspect ratio. Therefore, there is a need to obtain a framework to understand the behavior of PCM heat sink under varying conditions of thermal load, cut-off temperature, and geometry (aspect ratio) to determine the ideal configuration that is best suited for the given operating conditions.

As discussed in the literature review above, the dependence of the optimum PCM volume% on the simultaneous effect of boundary condition, cut-off temperature, and aspect ratio is not present in the literature regarding balancing the power density and the energy density for comparison between different cases. Even though material properties like volumetric latent heat and mass density can help estimate the amount of energy available in the PCM or PCM-filler composite based on mass and volume constraints, during the transient operation involving a temperature limit as a constraint, it becomes essential to understand the amount of latent energy accessed by the PCM at varying rates of heat supply, cut-off temperature, and geometry (aspect ratio/thickness). This research gap is the motivation behind the current work where an experimentally validated numerical model aids in generating power density vs. energy density, often referred to as the thermal Ragone chart, to determine the optimum balance of the power density and energy density of the composite for a given heat rate, aspect ratio, and cut-off temperature. Ragone plot was initially developed to characterize and compare the battery electrochemical energy storage [32]. The energy

delivered tends to reduce in batteries at high power levels. The PCM thermal energy storage is analogous to this behavior through a reduction in the energy stored in the PCM as the power is increased due to a limit in the thermal conductivity. Researchers have previously used this analogy to design and characterize thermal energy storage systems and PCM-based heat exchangers [10,33,34]. However, to the author's best knowledge, understanding the small-scale transient thermal energy storage in electronic cooling applications using Ragone framework is not in the literature.

In the present study, a thermal Ragone chart was explicitly used to design and compare the PCM-based heat sinks for transient thermal management of electronic devices. In the thermal buffering of the electronic components, the thermal performance can be highly dependent on the thermal boundary conditions, cut-off temperature, and geometry. For instance, the heat rate supplied to the thermal buffer may dictate the need for the enhancement of the thermal conductivity of the composite. The cut-off temperature or the maximum allowable temperature of the electronic device for its safe operation may also change the selection of the type of composite that can efficiently consume the amount of energy storage available in the PCM. The composite material's aspect ratio determines the resistance to attain maximum capacitance at a specific power level and cut-off temperature. Therefore, the performance metrics that are based on the intrinsic thermal properties of the composite, mainly the effective thermal conductivity and the adequate energy storage capacity, fail to consider the effect of the heat rate, cut-off temperature, and geometric aspect ratio to quantify the thermal performance under varying conditions of these parameters.

Furthermore, thermal Ragone plots were used in comparing various scenarios, such as (a) kind of phase change material (n-eicosane and gallium), (b) morphology of the porous foam (sintered particles and high porosity foams), (c) varying porosities of the foams. The two PCMs selected were based on the big difference in their thermal conductivity and volumetric latent heat but at a similar melting temperature so that they can be fairly compared for an application that demands a specified range of melting temperatures. The two kinds of porous foams were selected to consider a varying range in the porosity or PCM volume%. PCM volume in the 20 % to 80 % range is considered for the sintered particle porous foam. In contrast, the 88 % to 98 % range of PCM volume for the high porosity foams is evaluated based on their manufacturability.

2. Experimental setup and procedure

The experimental setup used in this study, as shown in Fig. 1(a), consists of a test module, a D.C. power supply (Keysight E3634A), a data acquisition system (Lab Jack T7), and a computer. The test module includes a polyimide heater (Omega, KHLVA-101/10) of 25 mm × 25 mm area attached to one side of a 2.5 mm thick copper base plate of the same area surrounded with Teflon for insulation. The copper foam and PCM are then placed in the vacant volume, as shown in Fig. 1(b) schematic. The test module is placed in a vacuum oven, heated for 30 mins at 45 °C for melting, and then cooled for 2–3 hrs for solidification to impregnate the PCM into the foam. After the impregnation, samples were analyzed using an optical microscope to ensure no large air pockets were present in the composite. The copper foam used in the experiment is 110 PPI (pores per inch) high porosity foam with a porosity of ∼ 97 % (MSE Supplies), and the organic PCM used is n-eicosane (Sigma Aldrich). The three-dimensional and scanning electron microscopy (SEM) images of the foam used are shown in Fig. 2(a) and Fig. 2(b), respectively. The height of the composite is 8 mm, and the mass of n-eicosane used was approximately 3.75 g. To record the temperatures during experiment tests, two calibrated T-type thermocouples (Omega, TT-T-36) with uncertainty of ± 0.5 °C were attached to the bottom and top sides of the PCM-foam composite using a thermal conducting epoxy. The constant voltage supply from the D.C. power supply unit controlled the desired power input to the heater. The transient experiments were performed at a constant heat rate, and the transient temperature response at the sample's bottom (heated side) and top (convection-cooled side) was recorded. The heater is turned off when the temperature reaches the cut-off temperature of 70 °C at the heating side. The PCM-foam composite is then allowed to cool by natural convection from the top side. Additional detail on the experiments and repeatability test can be found in supplementary document (Section S3).

2.1. Experimental results during heating and cooling

The time taken to reach the cut-off temperature (t_{cutoff}) is recorded for heat rate in the range of 2 W to 10 W with an increment of 1 W. The solidification time and the time to reach the cut-off temperature are also recorded. The heating is turned on until the temperature at the bottom side reaches the set cut-off temperature of 70 °C (stated as a cut-off point in further discussions). Fig. 3(a) and Fig. 3(b) depict the temperature during melting and solidification, respectively, of the PCM at selected five heat rate values. The melting behavior differs at different heat rates, as seen from the transient temperature curves during heating and solidification. It can be observed from Fig. 3(a), which depicts the heating phase, that when the cut-off temperature of 70 °C is reached on the heated side, only 2 W case has top side temperature above the PCM

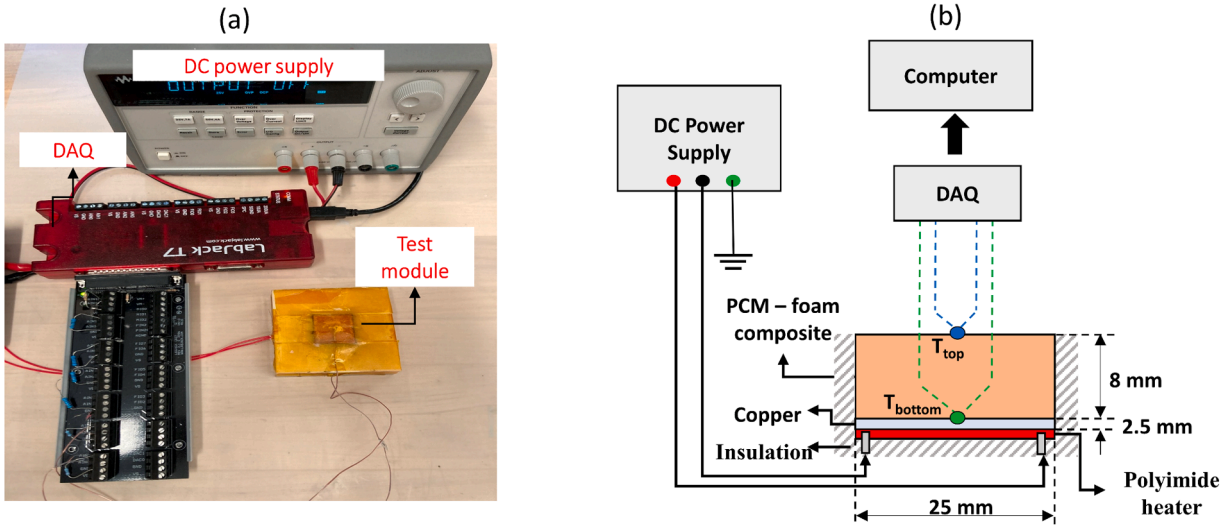

Fig. 1. (a) Experimental test setup used in the present study (b) schematic of the test module with dimensions.

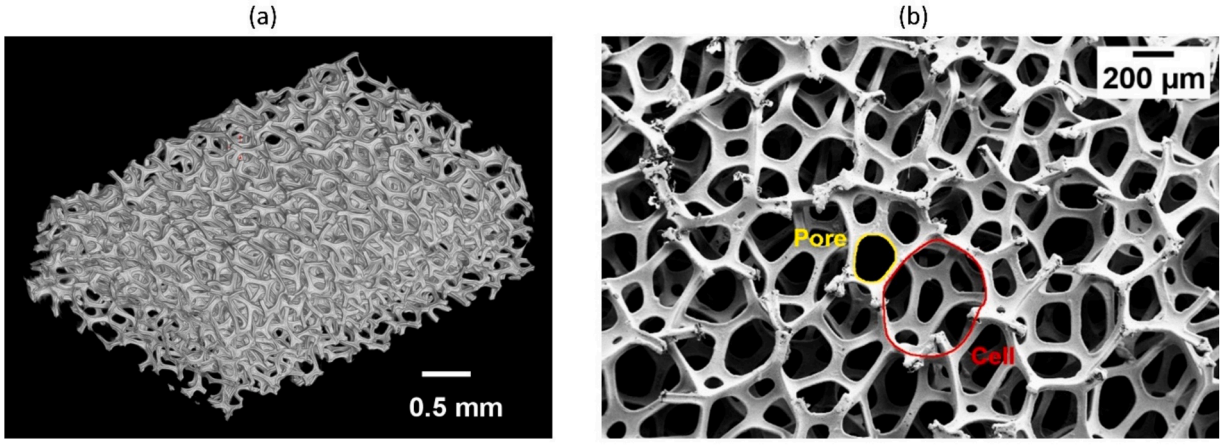

Fig. 2. (a) C.T. scan and (b) SEM image of the porous foam used in the present experiment.

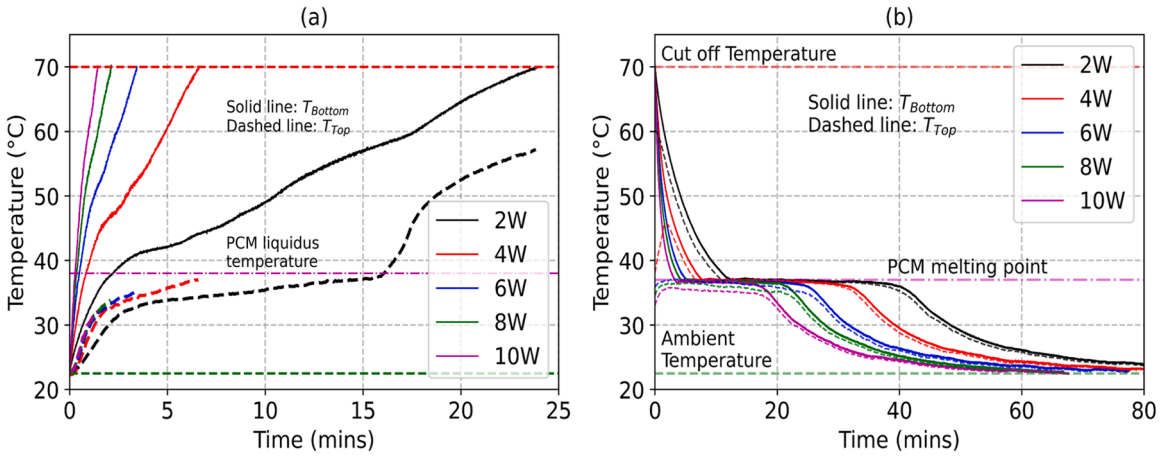

Fig. 3. (a) Heating (melting) phase, (b) Cooling (solidification) phase.

liquidus temperature. This indicates that complete PCM melting happens only in the case of 2 W heat input, with the temperature at the top side reducing at the cut-off as the heat rate increases. Also, this can be confirmed by the time taken during solidification at different heat rates in the cooling phase, as shown in Fig. 3(b), considering the time taken during solidification to indicate the amount of PCM melt during the heating phase. The time taken during the solidification continuously drops as the heat rate increases from 2 W to 10 W. The present 110 PPI foam and n-eicosane composite experiments were also used to validate the numerical model in Section 3.1. Though the temperature at the top and bottom side can provide information about whether the complete melting has happened, the exact amount of the PCM utilized until the cut-off point can only be determined if the temperature or enthalpy profile throughout the domain is known, which would require a large number of measurements experimentally. Therefore, a numerical model is needed to determine the enthalpy profile in the PCM at the cut-off point.

3. Numerical model and thermal Ragone plot

The numerical model was developed based on the heat conduction with the solid-liquid phase change in the PCM using the effective medium properties of the porous foam and PCM composite. The boundary conditions in the numerical model are constant heat flux at the bottom and a convection heat transfer coefficient of 10 W/m^2 K at the top. The top surface heat transfer coefficient is estimated using the correlation for natural convection over an isothermal horizontal flat plate [35]. The present numerical model ignores the fluid flow of the molten PCM and only solves the heat transport due to conduction and phase change. The effective heat capacity of the composite is obtained by volume averaging the heat capacity of the foam and the PCM. The effective thermal conductivity is obtained from the Boomsma and Poulikakos model [36]. The numerical model solves the energy equation for the transient heat conduction in the effective medium with the phase change term for the PCM melting and solidification. The numerical solution was obtained using a finite difference method with a central differencing scheme for spatial discretization and a semi-implicit Crank-Nicolson scheme for time marching [37]. The numerical model code was developed using MATLAB R2022a [38].

Governing energy equation:

$$\rho C_{eff}\frac{\partial T}{\partial t} = k_{eff}\left(\frac{\partial^2 T}{\partial x^2}+\frac{\partial^2 T}{\partial y^2}\right) - \varphi\rho_p L\frac{\partial \beta}{\partial t} \tag{1}$$

where,

$$\beta = \begin{cases} 1, & T \geq T_m + \varepsilon \\ 0, & T \leq T_m - \varepsilon \\ \dfrac{T-(T_m-\varepsilon)}{2\varepsilon}, & T_m - \varepsilon < T < T_m + \varepsilon \end{cases} \tag{2}$$

$$(\rho C)_{eff} = \varphi\cdot(\rho C)_{pcm} + (1-\varphi)\cdot(\rho C)_{cu} \tag{3}$$

Here, k_{eff} and ρC_{eff} are the effective thermal conductivity and effective

heat capacity of the composite, respectively. β represents the phase transformation fraction of the PCM, T_m is the melting temperature of the PCM, φ is the PCM volume fraction in the composite, L is the latent heat of PCM, and ε is a small number to define the temperature range of the phase change and taken as 0.5 in this study.

3.1. Validation of the numerical model

Fig. 4(a) shows the comparison between experiment and model values of the top temperature when the cut-off temperature of 70 °C at the bottom side is reached for all the heat rate values in the range of 2 W to 10 W. Additionally, the transient temperature at the top and bottom locations for heat rate of 5 W is compared with the experiment results to validate the model as shown in Fig. 4(b). The mean absolute error in the transient temperature between the experiment and numerical model at the bottom and top location was 5.51 % and 7.14 %, respectively. The mean absolute error in the top temperature at the cut-off point obtained in the experiment and numerical model in Fig. 4(a) was 1.73%. The present experimental results are also compared with a high-fidelity model developed on a commercially available solver (ANSYS Fluent 2022 R2 [39]) that considers the fluid flow and natural convection in the PCM and based on thermal non-equilibrium for the heat transfer at the foam and PCM interface. The governing equations and the model inputs for the high-fidelity model can obtained in the Supplementary document (Section S2). The high-fidelity model more accurately captures the transient temperature response when compared with the experimental observation with the mean absolute error at the bottom and top location of around 2.5 % and 2.8 %, respectively. The accuracy in the transient temperature obtained in the high-fidelity model is almost 2–3 times higher than the present model. Nonetheless, the error in the performance metric i.e., time to reach the cutoff temperature is similar in both the models as shown in Fig. 4(b) where the time to reach the cutoff temperature in the present and high-fidelity model is 7.7 % lower and 11.5 % higher than the experimental value, respectively. Additionally, despite the merit of the high-fidelity model in capturing the transient temperature response, the computation time is around 500 times higher than the present simplified model, making it computationally very expensive especially when a large quantity of simulations is required for comprehensive analysis.

The thermophysical properties of the PCMs used in the present study were considered as phase-dependent and temperature-independent and are shown below for the solid and liquid phase in Table 1. The thermophysical properties of copper used in the calculation of the effective medium properties were considered at 27 °C and were assumed as temperature independent.

3.2. Energy and power density calculation

The validated numerical model was then used to evaluate the change in enthalpy averaged over the thickness of the composite effective medium until the cut-off point is reached to find the amount of energy stored in the n-eicosane and 97 % copper foam composite and hence further used in calculating the volume and mass-based energy densities. Firstly, the temperature profile is obtained along the thickness direction, and based on the temperature, the enthalpy profile is obtained based on the predefined enthalpy change as a function of temperature shown in Fig. 5(b). Then, the enthalpy profile is averaged over the thickness and is denoted by $\overline{\Delta h}$. Fig. 5(a) shows the average enthalpy change obtained from the model (blue curve), representing that enthalpy change averaged over the computational domain at the cut-off point.

The averaged change in the enthalpy starts to become lower than the liquidus enthalpy change (complete melting) at the heat rate value of around 5 W (shown as a green square), indicating incomplete melting of the PCM at the cut-off point. The liquid fraction contour at different heat rates is added in Fig. 5(a), with 1 (red) and 0 (blue) representing the liquid and solid PCM, respectively. The enthalpy profile is obtained from the temperature as expressed in the following equation:

$$h_{v\ cutoff}(y) = \begin{cases} \rho C_{eff} T(y) + \rho_p L\varphi, & T(y) \geq T_m + \varepsilon \\ \rho C_{eff} T(y), & T(y) \leq T_m - \varepsilon \\ \rho C_{eff} T(y) + \rho_p L\varphi \left(\dfrac{T(y) - (T_m - \varepsilon)}{2\varepsilon} \right), & T_m - \varepsilon \leq T(y) \leq T_m + \varepsilon \end{cases} \tag{4}$$

$$\overline{h}_{v\ cutoff} = \frac{1}{l} \int_0^l h_{v\ cutoff}(y) \cdot dy \tag{5}$$

Here, $\overline{h}_{v\ cutoff}$ is defined as the average volumetric enthalpy over the domain when the cut-off point is reached. The value is calculated after finding the temperature profile at the cut-off point. Then, based on the temperature, the enthalpy profile is obtained and averaged along the thickness of the PCM or PCM composite, as shown in the following equation. Please note that h represents the specific enthalpy with unit J/g, whereas h_v is the volumetric enthalpy with unit J/m^3. Volumetric enthalpy is used for further calculations.

Moreover, $h_{v\ 0}$ is the enthalpy at the initial condition of temperature T_0.

$$h_{v\ 0} = \rho C_{eff} T_0 \tag{6}$$

Energy density (volume based):

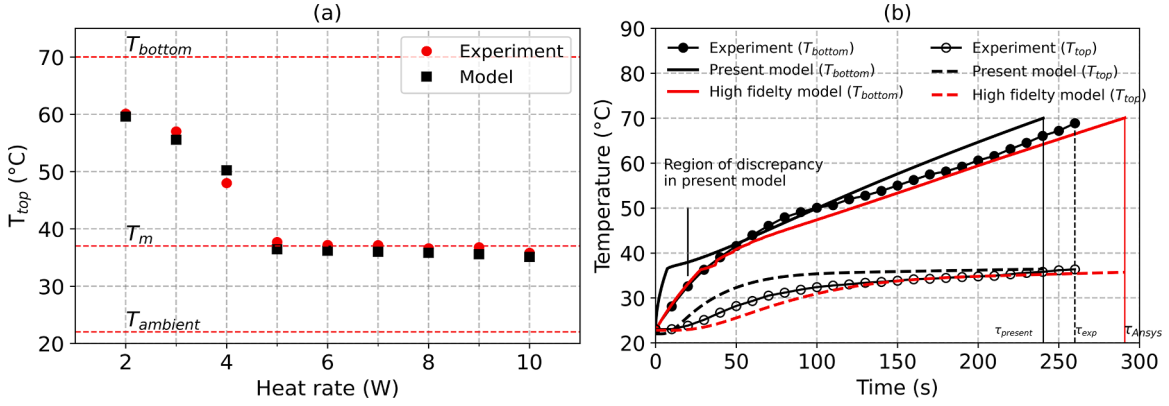

Fig. 4. (a) Comparison of experimental and model predicted top temperature at the cut-off, (b) Transient temperature comparison between the numerical model and experiment.

Table 1
Thermophysical properties of the materials used in the numerical model [11,40].

Material	Density (g/cm^3)	Thermal conductivity (W/m K)	Specific heat (J/g K)	Latent heat of fusion (J/g)	Melting Point (°C)
n-Eicosane	0.82 (solid) 0.78 (liquid)	0.212 (solid) 0.160 (liquid)	1.9 (solid) 2.2 (liquid)	237.4	37
Gallium	5.910 (solid) 5.907 (liquid)	40.6 (solid) 29.4 (liquid)	0.37 (solid) 0.37 (liquid)	80.1	29.8
Copper	8.91	398	0.385	–	–

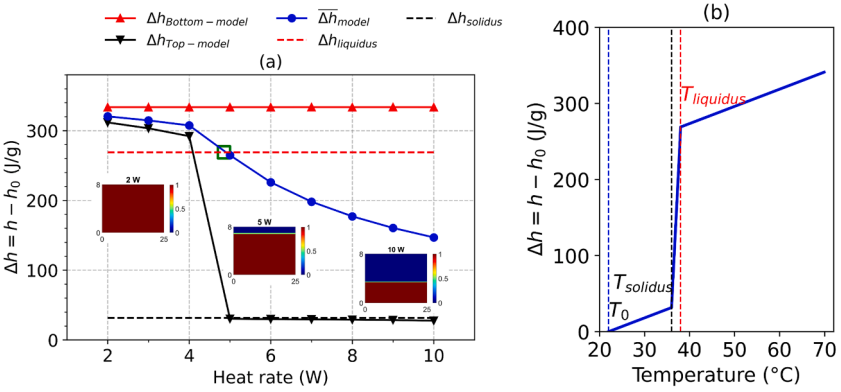

Fig. 5. (a) Enthalpy change obtained from the numerical model along with the PCM liquid fraction at different heat rates, (b) Enthalpy change as a function of temperature.

$$E_v = \left(\overline{h}_{v\ cutoff} - h_{v\ 0}\right)\left[\frac{J}{m^3}\right] \tag{7}$$

Power density (volume based):

$$P_v = \frac{q^{"}\cdot A}{V}\left[\frac{W}{m^3}\right] \tag{8}$$

Specific energy (mass-based energy density):

$$E_m = \frac{\left(\overline{h}_{v\ cutoff} - h_{v\ 0}\right)}{m} V\left[\frac{J}{g}\right] \tag{9}$$

Specific power (mass-based power density):

$$P_m = \frac{q^{"}\cdot A}{m}\left[\frac{W}{g}\right] \tag{10}$$

3.3. Thermal ragone plot

The thermal Ragone plot depicting the power density and energy density for the present n-eicosane-97 % porosity foam composite and pure n-eicosane is shown in Fig. 6(a) for a fixed total volume of 25 × 25 × 8 mm^3. The energy and power density values are calculated as described in equations 7 - 10. It is worth noting that the energy density is essentially the amount of the latent and sensible thermal energy stored in the PCM or PCM-foam composite until the cut-off point is reached. The vertical dashed lines represent the maximum energy storage capacity for the corresponding case. It is clear from the thermal Ragone plot that the pure n-eicosane has a lower power density than the composite of n-eicosane and 97 % porosity foam due to the lower thermal conductivity in the pure n-eicosane case. Even though the maximum energy storage capacity is high in the case of pure n-eicosane because of the higher amount of PCM for the same total volume, the actual energy density stored is lower. Adding copper foam removes 3 % of the PCM

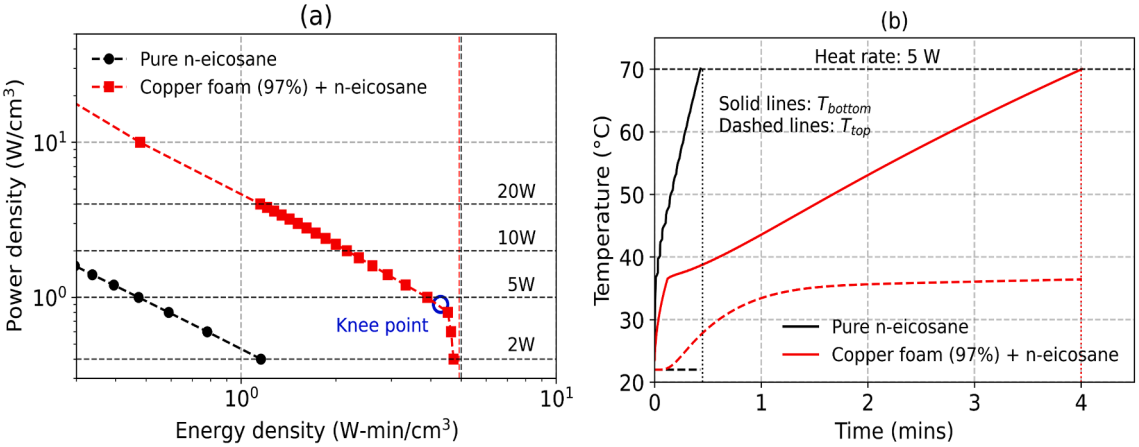

Fig. 6. (a) Thermal Ragone plot showing the power density vs. energy density and (b) Transient temperature at the bottom and top locations at a heat rate of 5 W for the pure n-eicosane and 97 % copper foam-eicosane composite.

volume, reducing the maximum energy storage capacity. Nevertheless, more net energy density is achieved due to the enhancement in the effective thermal conductivity of the composite.

It should be noted that the higher energy density at a given power level dictates the time to reach the cut-off temperature, as depicted in Fig. 6(b). The n-eicosane-97 % porosity copper foam composite has a higher energy density than pure n-eicosane at all power density values. However, the balance between the power density and the energy density can be more competitive when a different material or porosity of the foam is used. An intersection in two different curves can dictate the choice of the material/porosity/type of porous foam to be used that maximizes the energy density at a given heat rate and maximizes the time to reach the cut-off temperature.

Also, as the power density is increased, energy density tends to reduce, and beyond a certain point (knee point), there is a drastic reduction in the energy density. The knee point represents the point at which the complete melting of PCM is not achieved at the cut-off temperature as the power density increases. Fig. 6(a) indicates the knee point as a blue circle for the n-eicosane-97 % porosity copper foam composite. In the forthcoming discussions, it is crucial to emphasize that the available energy density remains constant across various cases under consideration. Our study does not aim to augment the available energy density of the PCM composite, a critical constraint that enhances its relevance to electronic cooling applications. However, the pivotal distinction lies in identifying the optimal design that maximizes the accessed energy density within this fixed available energy density for various operating conditions, distinguishing our study from existing literature.

4. Results and discussions

4.1. Effect of pcm and porous media

The power and energy density obtained from the numerical model are used to generate a thermal Ragone plot for comparative analysis. The PCMs used in this analysis are n-eicosane ($T_m = 37$ °C) and gallium ($T_m = 29.6$ °C), selected to consider a significant variation in their thermal conductivity and latent heat with similar melting points. The porous media used in the analysis are open-celled, high-porosity copper foams and sintered copper particle foam. The present study lists six cases with properties in Table 2. The effective thermal conductivity of the high porosity copper foams and sintered foams are obtained using the model by Boomsma and Poulikakos [36] and Alexander [41], respectively. The detailed calculation of the effective thermal conductivity can be found in Supplementary document (Section S1). The effective volumetric latent heat storage capacity (L_{eff}) in Table 2 is the product of the volumetric latent heat of the PCM and the porosity of the foam (PCM volume%).

Table 2
The cases considered for comparison in the thermal Ragone plot.

Case	Label	Remarks		φ (-)	k_{eff} (W/m K)	L_{eff} (J/cm^3)
		PCM	Porous media			
1	n – E 100 % (Pure n-eicosane)	n-eicosane	N/A	1	0.15	190
2	n – E 97 % (Present)	n-eicosane	High porosity foam	0.97	1.74	184.3
3	n – E 88 %	n-eicosane	High porosity foam	0.88	4.31	167.2
4	n – E 80 %	n-eicosane	Sintered particles	0.80	4.25	152
5	n – E 55 %	n-eicosane	Sintered particles	0.55	25	104.5
6	Ga 100 % (Pure gallium)	Gallium	N/A	1	40.6	486.4

4.1.1. Fixed volume constraint

For the cases mentioned in Table 2, thermal Ragone plots are obtained based on fixed volume and fixed mass of the PCM/PCM-porous media composite as the constraints. The total volume is set as 25 × 25 × 8 mm^3 in the fixed volume constraint. The plot shown in Fig. 7(a) depicts the thermal Ragone plot for a fixed volume of all the cases at the cut-off temperature of 70 °C. The vertical dashed lines represent the maximum accessible energy density in the corresponding cases and include the total latent and sensible energy available until the cut-off temperature. The ideal case will be to reach the maximum available energy density and higher power density simultaneously with fixed total volume as a constraint. However, in the cases of high PCM volume% based on n-eicosane such as n-E (100 %), n-E (97 %), and n-E (88 %), due to their relatively low effective thermal conductivity, there is a knee point at lower values of heat rate and the energy density starts to reduce drastically as the power density (heat rate) is increased beyond the knee point. In the case of gallium and n-E (55 %), the high effective thermal conductivity values help keep the knee point at a higher power density. Therefore, at a low power density value of 2 W, most of the energy storage capacity is utilized in all cases except the 100 % eicosane case. As the power density increases, energy density deviates from the maximum value, as depicted in Fig. 7(b), showing the actual energy density accessed and the maximum energy density available (unfilled bars with dashed border). The knee point rises to higher power density as the effective thermal conductivity increases.

For example, at the power density corresponding to the heat rate of 5 W, the energy density in the n-E (97 %) case deviates from the maximum energy density. Whereas, for the n-E (88 %) case, the knee point is approximately at the power density corresponding to a 10 W heat rate. Hence, for heat rates up to 5 W, both the n-E (97 %) and n-E (88 %) cases have nearly the same energy density; however, for heat rates higher than 5 W, the n-E (88 %) case has higher energy density at a given power density. Fig. 8 depicts the temperature vs. time during the melting of the PCM at the cut-off point for different heat rate values selected based on the points of intersection between different curves in the thermal Ragone plot. Fig. 8(b) indicates one of such intersection points between red and green curves for clarification. It can be seen that gallium takes the most extended amount of time to reach the cut-off temperature irrespective of the heat rate values because of their almost vertical behavior in the energy density. For the cases with n-eicosane as the PCM (cases 1 to 5 in Table 2) there are some power density values at which intersections are happening.

This is demonstrated in the temperature vs time plots at 5 W, 10 W, and 20 W, where the reader should ignore gallium for clarity in comparing the cases based on n-eicosane as PCM. As shown in Fig. 8(a), (b), and (c), the n-E (88 %) case takes the longest time to reach the cut-off temperature among the cases with n-eicosane as PCM. However, for a heat rate of more than 12.5 W, n-E (55 %) has the highest energy density and hence takes the longest time to reach the cut-off temperature, as shown in Fig. 8(d), showing the transient temperature plot at a heat rate of 20 W. Therefore, the temperature–time plots are consistent with the variation in the thermal Ragone plot. The time obtained to reach the cut-off temperature for all the cases is shown in Fig. 8(e), with the red shaded portion zoomed and displayed on the right side for clarity to look at the intersection points. The thermal Ragone plot obtained signifies power and energy density behavior based on a fixed volume available for the composite or pure PCM. This information can enable the designer to compare different cases to obtain the case with the maximum energy density at a known power density or vice versa.

As this thermal Ragone plot is based on the fixed volume as the constraint, it is expected that the material or the composite medium with the highest value of the volumetric energy density available should be the ideal case. However, as the maximum temperature limit is selected as a constraint (cut-off point), the amount of energy stored (accessed energy density) in the material or composite becomes a more significant parameter than the available energy density.

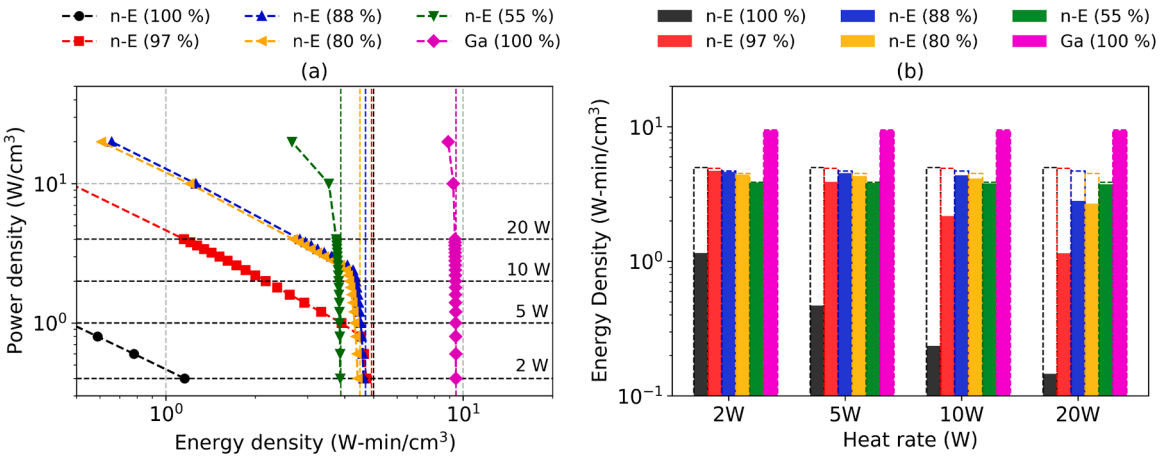

Fig. 7. (a) Power density vs. energy density for fixed volume (25 × 25 × 8 mm^3) constraint, (b) Energy density consumed and the energy density available at different heat rates.

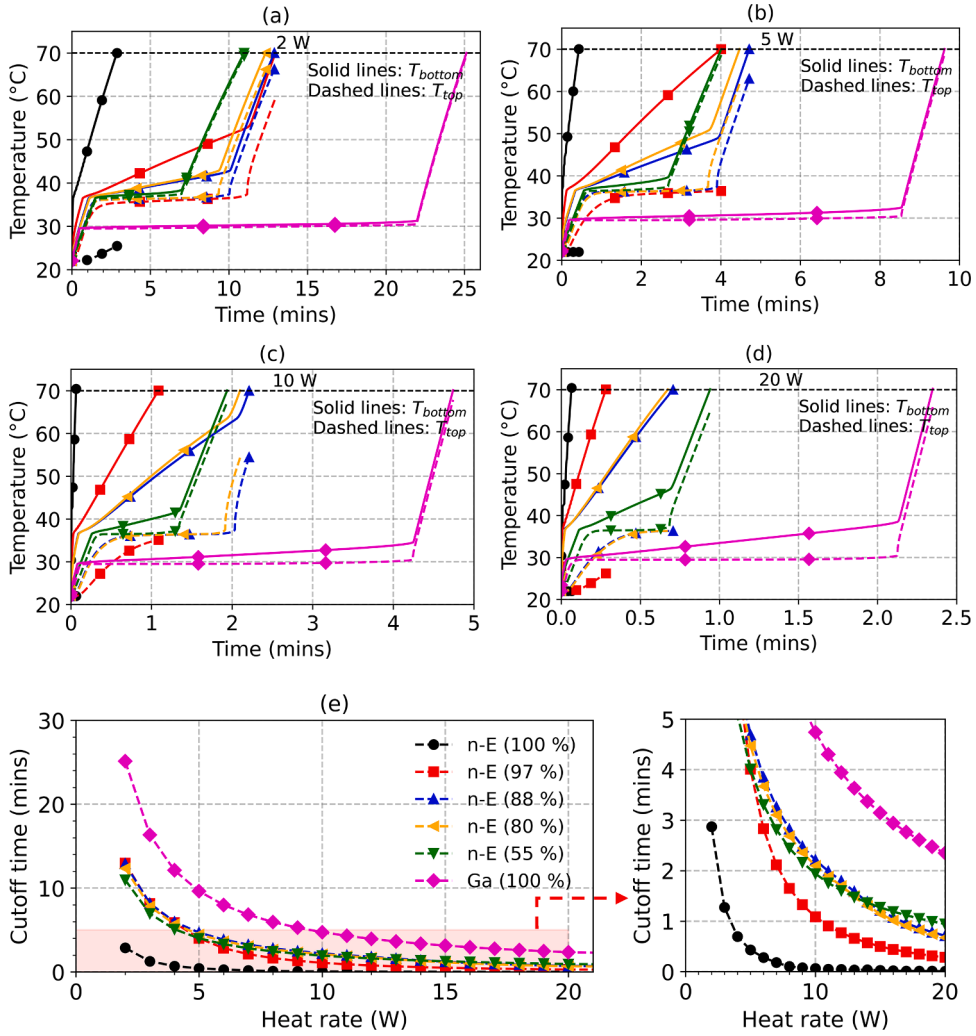

Fig. 8. Temperature vs. time at (a) 2 W, (b) 5 W, (c) 10 W, (d) 20 W, and (e) Time to reach the cut-off temperature of 70 °C with the plot on the right showing the shaded zone for clarity (Note: Solid and dashed lines in (a) – (d) represent the temperature at the bottom and top locations, respectively).

Moreover, as seen in Fig. 7, the energy density can be highly dependent on the rate at which the heat is supplied to the PCM. In the fixed volume constraint, it is clear that the gallium has the highest volumetric energy density in addition to the high thermal conductivity value. However, the major demerit is the high mass density of gallium, which makes it six times heavier than the n-E (97 %) case for the same volume. This is a significant concern, especially for portable and hand-held electronic devices where the mass occupied by the cooling module

needs to be lower with/without the limit on the volume occupied. Therefore, fixed mass is also considered a constraint and discussed in the next section.

4.1.2. Fixed mass constraint

In the fixed volume constraint, the case with the most significant volumetric energy density at a given power density will always take the longest to reach a cut-off temperature of 70 °C, as discussed in the previous section. However, it is also important to note that higher mass density is a demerit in most portable electronic devices by causing more weight to the cooling module. Therefore, a comparison based on the fixed mass of the composite is needed. This section considers a fixed mass of 5 g for all the cases mentioned in Table 2. The power density and energy density are represented here as specific power and specific energy, respectively, to avoid confusion. The thermal Ragone plot in Fig. 9 (a) depicts the five cases' specific power vs. specific energy. For specific power, less than 1.6 W/g, i.e., a heat rate of around 8 W, n-E (97 %) consumes the highest specific energy until the cut-off temperature is reached.

Additionally, Fig. 9(b) shows the energy density accessed until the cut-off point and the maximum energy density available for the fixed mass constraint. However, at a specific power higher than 1.6 W/g, the n-E (88 %) case has a higher specific energy. Therefore, in the transient temperature plot, n-E (97 %) case took the longest time to reach the cut-off point at the heat rate values of 2 W and 5 W, as shown in Fig. 10(a) and (b). In Fig. 10(c), as the heat rate increases to 10 W, the n-E (88 %) performs better as the energy density and time to reach the cut-off temperature is higher than the n-E (97 %) case. Fig. 10(d) shows the cut-off time vs. heat rate for the cases considered.

Overall, the significant point in the thermal Ragone plot based on the mass constraint depicts the change in the optimal case (intersection of blue and red curves) when the heat rate was higher than 8 W, as shown in Fig. 9(a).

4.2. Effect of foam porosity or PCM volume%

The two kinds of porous media considered in the previous section were used in this section with the detailed variation in the volume% of the PCM. The high porosity open-celled porous foams and sintered copper powder are considered for PCM volume% in the 88 % to 98 % and 20 % to 80 %, respectively. The porous media are simulated in the specified range of the PCM volume% for fixed volume and fixed mass constraint.

As mentioned in the previous sections, a fixed total volume of 25 × 25 × 8 mm^3 is considered for the PCM-foam composite in the specified volume constraint. Fig. 11(a) depicts the power density versus the energy density for the high porosity foams at different PCM volume%. At the low heat rate values, accessed energy density is almost the same for all the PCM volume% values; however, as the heat rate increases, a higher energy density is observed for the high thermal conducting composites. This indicates that as the power density increases, adding the metal foam volume to enhance the thermal conductivity is more prominent in improving the accessed energy density for the fixed total volume. Fig. 11(b) shows a similar trend for the sintered particle foams. As the power density increases, knee points are observed for each PCM volume%. The deviation from the available energy density increases the porous metal volume% to access more energy density. From the charts shown in Fig. 11, the locus of the maximum energy density can be used to determine the best volume% of PCM required to achieve the maximum cut-off time at a given heat rate value.

For the fixed mass constraint of 5 g, the specific power vs specific energy ranges plots depicted in Fig. 12(a) (for high porosity foams) and Fig. 12(b) (for sintered foams) show the behavior at different heat rates.

The knee points indicate that a particular PCM volume% is no more useful if there is a drop in its specific energy as the other value of PCM volume% may achieve higher specific energy even though the total available energy storage is lower in the latter case. The specific power and specific energy curves for the sintered foams shown in Fig. 12(b) are almost vertical for most of the PCM volume% values; this is due to the fixed mass taken as the constraint, which makes the composite very thin in the heat flow direction and therefore leads to the high value of the thermal conductance. Thus, the knee points will exist at a very high value of the specific power.

In this section, the PCM volume% of individual copper foams varied in the range typically manufactured in real applications. The locus of the points can be obtained based on the maximum energy density or specific energy points in the thermal Ragone curve for further utilization in determining the best case. Such charts can help find the optimal value of PCM volume% or porosity of the foam that maximizes the energy density at a desired power energy or vice versa.

4.3. Effect of cut-off temperature

The effect of different cut-off temperatures on the energy density and power density is shown in Fig. 13(a) for cases 1 to 5 mentioned in Table 2 for a fixed volume of 25 × 25 × 8 mm^3. All the curves shift to the left side due to reduced total energy storage with the knee points shifting down. The decrease in the energy density is more in the cases of n-E (100 %) and n-E (97 %) due to the compromised PCM latent heat storage as the cut-off temperature is reduced. However, in the case of n-E (55 %) with high effective thermal conductivity, dependence on energy storage as latent heat is significantly higher than sensible energy storage.

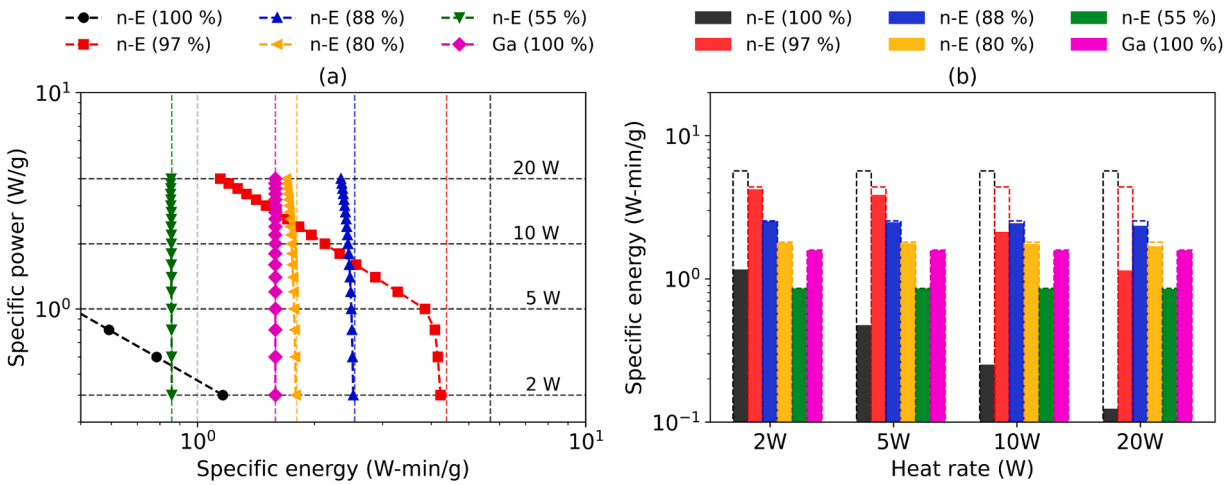

Fig. 9. Specific power vs specific energy for fixed mass (5 g) constraint.

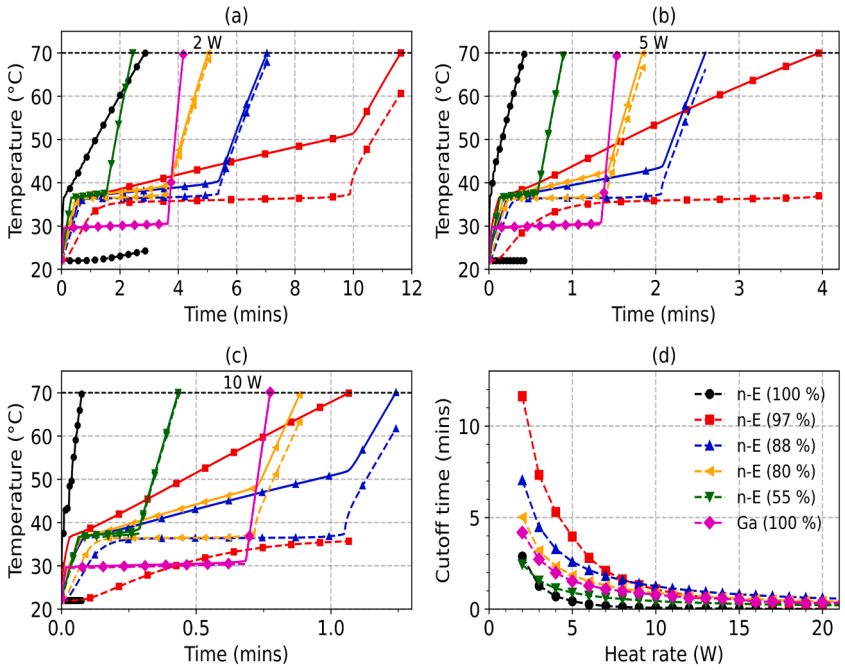

Fig. 10. Temperature vs time at (a) 2 W, (b) 5 W, (c) 10 W, and (d) Time to reach the cut-off temperature of 70 °C (Note: Solid and dashed lines in (a) – (d) represent the temperature at the bottom and top locations, respectively).

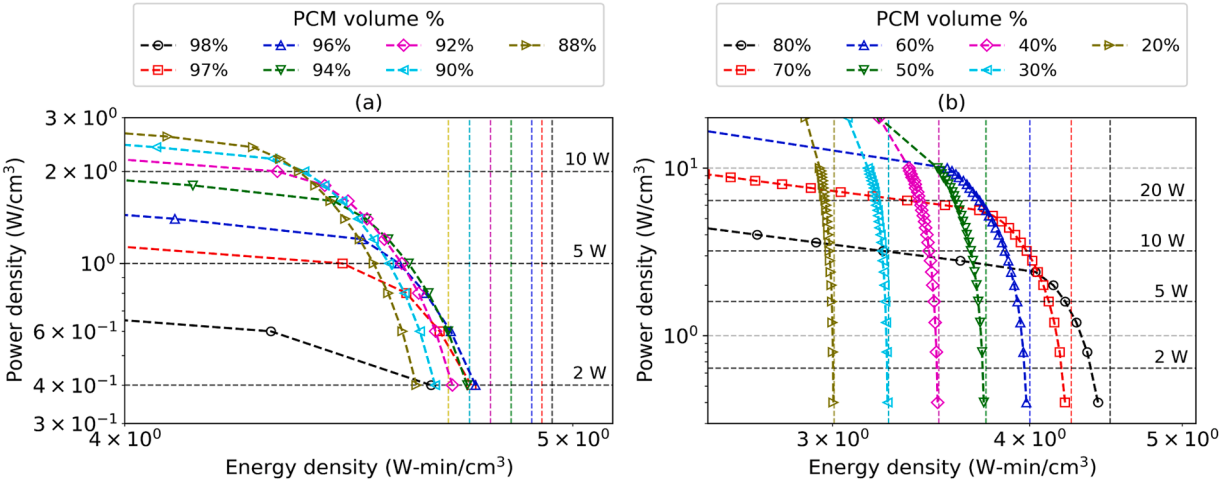

Fig. 11. Power density vs energy density for varying PCM volume% for (a) high porosity foam, (b) Sintered particles foam, and n-eicosane composite under a fixed volume constraint.

Therefore, the n-E (55 %) case is relatively less sensitive to the cut-off temperature, though at high power density, there is some reduction in the energy density. At heat rates of 2 W (low heat rate) and 20 W (high heat rate), the energy density is obtained in Fig. 13(a) at the cut-off temperatures of 45 °C (low cut-off) and 70 °C (high cut-off) to depict the effect of the cut-off temperature at different levels of power density as shown in the bar charts in Fig. 13(b). At a high heat rate, n-E (55 %) with sintered particle foam has the highest energy density, irrespective of the cut-off temperature. In contrast, at a low heat rate, n-E (88 %) and n-E (97 %) have the highest energy density at 45 °C and 70 °C cut-off temperatures, respectively.

4.4. *Effect of composite thickness (aspect ratio)*

To understand the effect of the geometric aspect ratio of the PCM or PCM composite on the energy density, cases 1 to 5 in Table 2 were used to obtain the power density and energy density for thickness values of 8 mm, 15 mm, and 25 mm for fixed footprint area of 25 × 25 mm^2. Fig. 14 (a), (b), and (c) depicts the thermal Ragone plot for different values of the composite thickness. It can be observed that the energy vs. power density trends are similar in all the thicknesses; however, the knee point, as well as the curve itself, shifts to lower power density as the thickness is increased. As the thickness increases, the thermal conductance reduces, and the energy density decreases for a fixed power density value. The amount of the energy density stored and the maximum energy density available in the composite is shown in Fig. 14(d). It is evident from Fig. 14(d) that the energy accessed by the composite is changed negligibly in the n-E (55 %) sintered foam as the thickness is increased.

In both bar plots shown in Fig. 14(b) and Fig. 14(d), it is evident that the overall available energy density remains consistent across all cases. However, the optimal scenarios manifest the highest accessed energy density, underscoring the framework's ability to uphold a constant

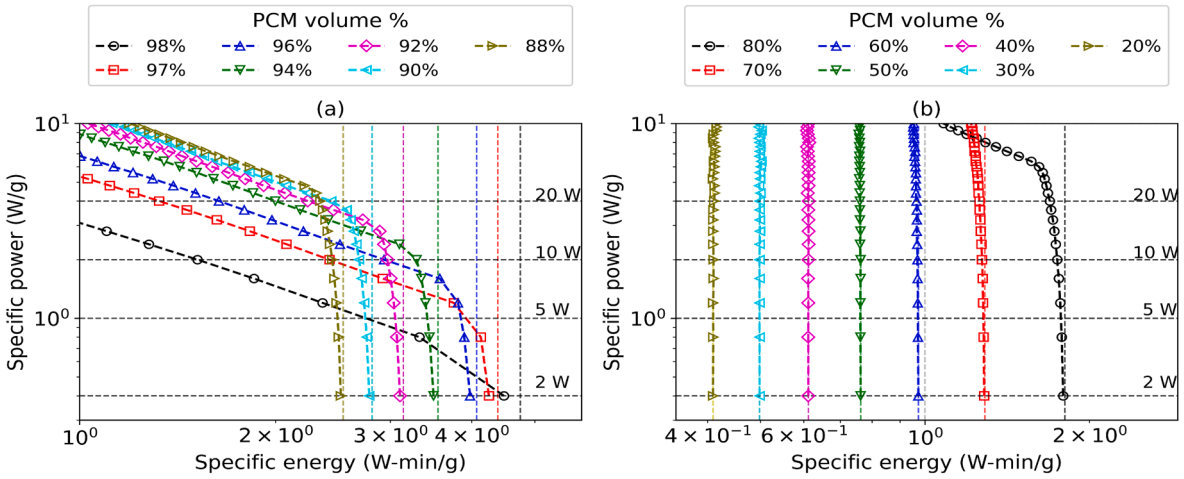

Fig. 12. Specific power vs specific energy for varying PCM volume% for high porosity foam and n-eicosane composite under fixed mass constraint.

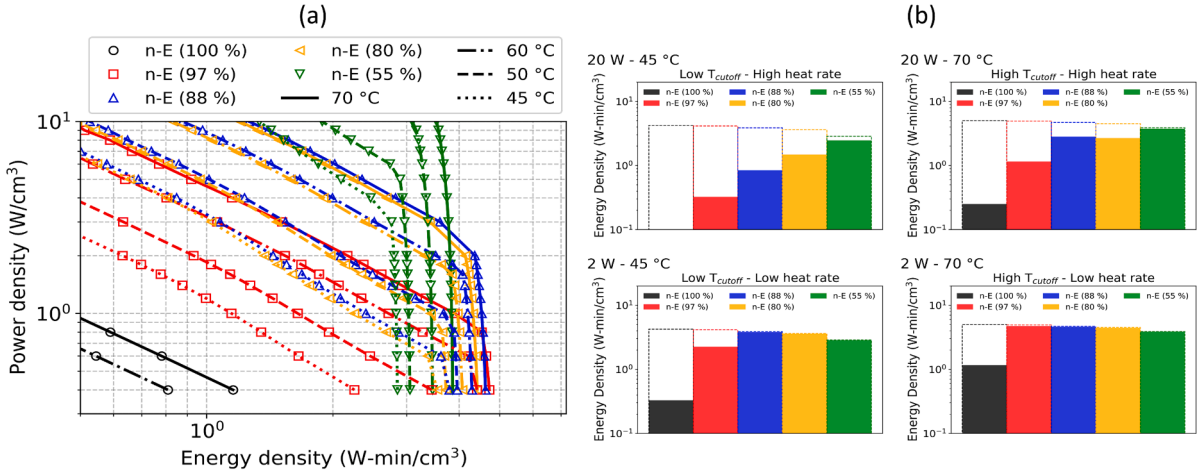

Fig. 13. (a) Power density vs energy density for fixed volume at different cut-off temperatures (b) Energy density at different cut-off temperatures and heat rate levels.

constraint of maximum available energy density while facilitating enhanced accessed energy density in optimal cases.

5. Conclusions

In conclusion, this research has effectively combined detailed experimental examinations and numerical simulations to investigate the transient thermal management of electronics using phase change materials (PCM). The comprehensive study demonstrated the development of a framework based on thermal Ragone plots derived from a benchmark numerical model (validated for 97 % porosity copper foam with a high pore density of 110 PPI impregnated with n-eicosane.) to unveil valuable insights into the design of PCM-based composites under varying boundary conditions and aspect ratios. These findings hold significant promise for advancing thermal management strategies in electronic devices, offering a robust foundation for optimizing PCM-based systems for enhanced performance and efficiency. The thermal Ragone framework is introduced as an effective tool for comprehending the principles governing the design of PCM-based composites, offering valuable insights for efficient and optimized thermal management solutions.

The key conclusions from the research study are as follows:

- The heat input rate, the cut-off temperature, and the aspect ratio (thickness) influence the selection of the porosity of the copper foam. Under fixed volume constraint, when the cut-off temperature is closer to the melting temperature of the PCM, low PCM volume% (high thermal conductivity) is favorable with n-E 55 % showing 2.9 times higher energy density than n-E (88 %) case, highlighting the importance of enhanced thermal transport within PCM-based composites. However, when the cut-off temperature is farther away than the melting temperature, at high power density, the difference in energy density becomes relatively less distinct between low and high PCM volume% where energy density is 1.32 times higher in n-E (55 %) than n-E (88 %), whereas at low power density, energy density is indistinguishable. This indicates a diminishing difference in performance (maximum energy density) across the various PCM volume percentages investigated at high cut-off temperatures.
- The increase in thickness necessitates additional filler metal volume to minimize thermal resistance and maximize thermal capacitance, as evidenced by the Ragone framework. In contrast, decreased thickness yields similar accessed energy densities across different PCM composite designs.
- Furthermore, under fixed mass constraint, a low PCM volume of 88 % in the high-porosity foam performed better under high power density, whereas a 97 % PCM volume performed better under low

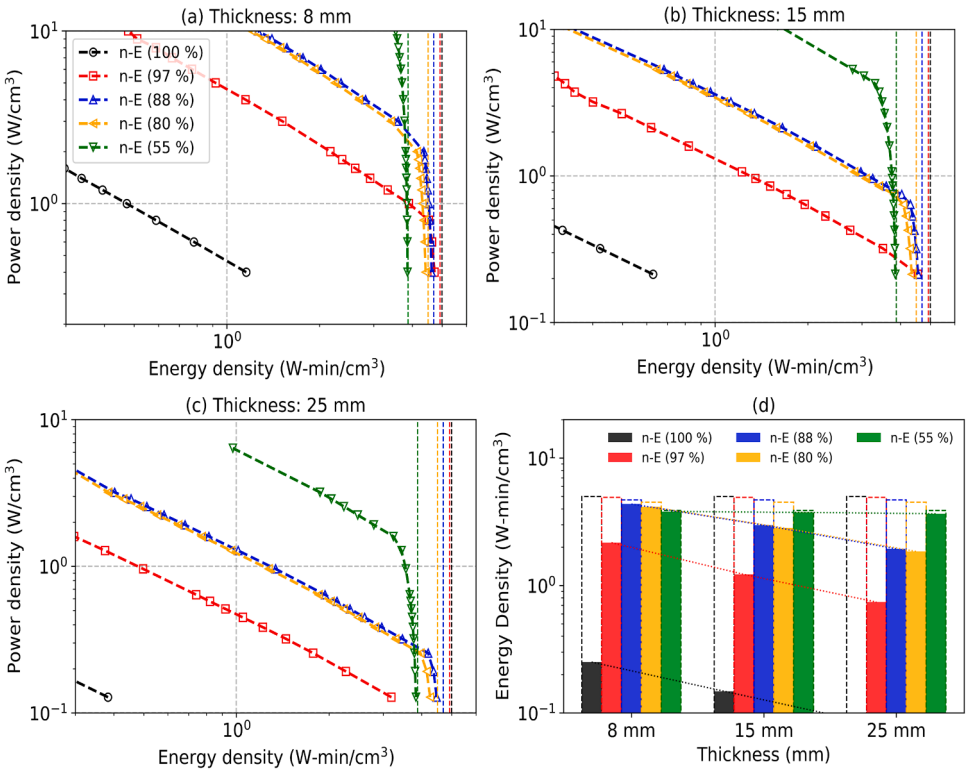

Fig. 14. Effect of composite thickness/aspect ratio for thickness (a) 8 mm, (b) 15 mm, (c) 25 mm, (d) energy density accessed vs energy density available at 10 W heat rate and 70 °C cut-off temperature.

power. However, it is also observed from the thermal Ragone plot (under fixed mass constraint) that the inherently low gravimetric latent heat of gallium impedes the accessibility of specific energy, whereas the high thermal conductivity and volumetric latent heat aids in higher energy density in the power density range considered in the study.

- The proposed framework employing thermal Ragone plots developed for a wide range of porosity of high-porosity (88 % to 98 %) and sintered particle foam (20 % to 80 %) demonstrates the behavior of the power and energy density. It can help designers find the PCM volume% that maximizes the energy density at a given power density or vice versa.

Overall, the thermal Ragone plots can help determine the optimal foam porosity/PCM volume% for various combinations of heat rate, cut-off point, and aspect ratio.

CRediT authorship contribution statement

Ayushman Singh: Writing – review & editing, Writing – original draft, Validation, Software, Resources, Methodology, Investigation, Formal analysis, Conceptualization. **Srikanth Rangarajan:** Writing – review & editing, Writing – original draft, Visualization, Validation, Supervision, Software, Resources, Project administration, Methodology, Investigation, Funding acquisition, Formal analysis, Data curation, Conceptualization. **Bahgat Sammakia:** Writing – review & editing, Writing – original draft, Visualization, Validation, Supervision, Software, Resources, Project administration, Methodology, Investigation, Funding acquisition, Formal analysis, Data curation, Conceptualization.

Declaration of competing interest

The authors declare that they have no known competing financial interests or personal relationships that could have appeared to influence the work reported in this paper.

Data availability

No data was used for the research described in the article.

Acknowledgment

This work was supported by Semiconductor Research Corporation CHIRP (Task 2878.015).

Supplementary materials

Supplementary material associated with this article can be found, in the online version, at doi:10.1016/j.ijheatmasstransfer.2024.125518.

References

[1] D. Zhou, C.Y. Zhao, Y. Tian, Review on thermal energy storage with phase change materials (PCMs) in building applications, Appl. Energy 92 (2012) 593–605, https://doi.org/10.1016/j.apenergy.2011.08.025.
[2] Y.H. Huang, W.L. Cheng, R. Zhao, Thermal management of Li-ion battery pack with the application of flexible form-stable composite phase change materials, Energy Convers. Manage 182 (2019) 9–20, https://doi.org/10.1016/j.enconman.2018.12.064.
[3] R. Kandasamy, X.Q. Wang, A.S. Mujumdar, Application of phase change materials in thermal management of electronics, Appl. Therm. Eng. 27 (2007) 2822–2832, https://doi.org/10.1016/j.applthermaleng.2006.12.013.
[4] T. Yang, J.G. Kang, P.B. Weisensee, B. Kwon, P.V. Braun, N. Miljkovic, W.P. King, A composite phase change material thermal buffer based on porous metal foam and low-melting-temperature metal alloy, Appl. Phys. Lett. 116 (2020) 071901, https://doi.org/10.1063/1.5135568.
[5] M.T. Barako, S. Lingamneni, J.S. Katz, T. Liu, K.E. Goodson, J. Tice, Optimizing the design of composite phase change materials for high thermal power density, J. Appl. Phys. 124 (2018) 145103, https://doi.org/10.1063/1.5031914.
[6] C. Nelson, J. Galloway, Package thermal challenges due to changing mobile system form factors, in: Proceedings of the 34th Thermal Measurement, Modeling &

Management Symposium (SEMI-THERM), San Jose, CA, IEEE, 2018, pp. 98–106, https://doi.org/10.1109/SEMI-THERM.2018.8357359.
[7] M.K. Berhe, Ergonomic Temperature Limits For Handheld Electronic Devices, American Society of Mechanical Engineers Digital Collection, 2010, pp. 1041–1047, https://doi.org/10.1115/IPACK2007-33873.
[8] A. Sharma, V.V. Tyagi, C.R. Chen, D. Buddhi, Review on thermal energy storage with phase change materials and applications, Renew. Sustain. Energy Reviews 13 (2009) 318–345, https://doi.org/10.1016/j.rser.2007.10.005.
[9] X. Xiao, P. Zhang, M. Li, Effective thermal conductivity of open-cell metal foams impregnated with pure paraffin for latent heat storage, Int. J. Therm. Sci. 81 (2014) 94–105, https://doi.org/10.1016/j.ijthermalsci.2014.03.006.
[10] J. Woods, A. Mahvi, A. Goyal, E. Kozubal, A. Odukomaiya, R. Jackson, Rate capability and Ragone plots for phase change thermal energy storage, Nat. Energy 6 (2021) 295–302, https://doi.org/10.1038/s41560-021-00778-w.
[11] Y. Liu, R. Zheng, J. Li, High latent heat phase change materials (PCMs) with low melting temperature for thermal management and storage of electronic devices and power batteries: critical review, Renew. Sustain. Energy Rev. 168 (2022) 112783, https://doi.org/10.1016/j.rser.2022.112783.
[12] H.M.Ali Tauseef-ur-Rehman, M.M. Janjua, U. Sajjad, W.M. Yan, A critical review on heat transfer augmentation of phase change materials embedded with porous materials/foams, Int. J. Heat. Mass Transf. 135 (2019) 649–673, https://doi.org/10.1016/j.ijheatmasstransfer.2019.02.001.
[13] A. Singh, S. Rangarajan, L. Choobineh, B. Sammakia, Figure of merit-based optimization approach of phase change material-based composites for portable electronics using simplified model, J. Electron. Packag. 144 (2021), https://doi.org/10.1115/1.4052074.
[14] A. Singh, S. Rangarajan, L. Choobineh, B. Sammakia, Thermal management of electronics during continuous and intermittent operation mode employing phase change material-based heat sinks—numerical study, IEEE Trans. Compon. Packag. Manuf. Technol. 11 (2021) 1783–1791, https://doi.org/10.1109/TCPMT.2021.3108054.
[15] P. Zhang, Z.N. Meng, H. Zhu, Y.L. Wang, S.P. Peng, Melting heat transfer characteristics of a composite phase change material fabricated by paraffin and metal foam, Appl. Energy 185 (2017) 1971–1983, https://doi.org/10.1016/j.apenergy.2015.10.075.
[16] C.Y. Zhao, Review on thermal transport in high porosity cellular metal foams with open cells, Int. J. Heat. Mass Transf. 55 (2012) 3618–3632, https://doi.org/10.1016/j.ijheatmasstransfer.2012.03.017.
[17] X. Meng, L. Yan, J. Xu, F. He, H. Yu, M. Zhang, Effect of porosity and pore density of copper foam on thermal performance of the paraffin-copper foam composite Phase-Change Material, Case Stud. Therm. Eng. 22 (2020) 100742, https://doi.org/10.1016/j.csite.2020.100742.
[18] V.V. Calmidi, R.L. Mahajan, Forced Convection in High Porosity Metal Foams, J. Heat. Transfer. 122 (2000) 557–565, https://doi.org/10.1115/1.1287793.
[19] S.S. Sundarram, W. Li, The effect of pore size and porosity on thermal management performance of phase change material infiltrated microcellular metal foams, Appl. Therm. Eng. 64 (2014) 147–154, https://doi.org/10.1016/j.applthermaleng.2013.11.072.
[20] A. Hussain, I.H. Abidi, C.Y. Tso, K.C. Chan, Z. Luo, C.Y.H. Chao, Thermal management of lithium ion batteries using graphene coated nickel foam saturated with phase change materials, Int. J. Therm. Sci. 124 (2018) 23–35, https://doi.org/10.1016/j.ijthermalsci.2017.09.019.
[21] L.W. Fan, Y.Y. Wu, Y.Q. Xiao, Y. Zeng, Y.L. Zhang, Z.T. Yu, Transient performance of a thermal energy storage-based heat sink using a liquid metal as the phase change material, Appl. Therm. Eng. 109 (2016) 746–750, https://doi.org/10.1016/j.applthermaleng.2016.08.137.
[22] T. Rehman, H.M. Ali, Experimental investigation on paraffin wax integrated with copper foam based heat sinks for electronic components thermal cooling, Int. Commun. Heat Mass Transfer 98 (2018) 155–162, https://doi.org/10.1016/j.icheatmasstransfer.2018.08.003.
[23] Z. Liu, Y. Yao, H. Wu, Numerical modeling for solid–liquid phase change phenomena in porous media: shell-and-tube type latent heat thermal energy storage, Appl. Energy 112 (2013) 1222–1232, https://doi.org/10.1016/j.apenergy.2013.02.022.
[24] Y. Tian, C.Y. Zhao, A numerical investigation of heat transfer in phase change materials (PCMs) embedded in porous metals, Energy 36 (2011) 5539–5546, https://doi.org/10.1016/j.energy.2011.07.019.
[25] R. Srikanth, C. Balaji, Experimental investigation on the heat transfer performance of a PCM based pin fin heat sink with discrete heating, Int. J. Therm. Sci. 111 (2017) 188–203, https://doi.org/10.1016/j.ijthermalsci.2016.08.018.
[26] T. Rehman, H.M. Ali, A. Saieed, W. Pao, M. Ali, Copper foam/PCMs based heat sinks: an experimental study for electronic cooling systems, Int. J. Heat. Mass Transf. 127 (2018) 381–393, https://doi.org/10.1016/j.ijheatmasstransfer.2018.07.120.
[27] T. Ahmed, M. Bhouri, D. Groulx, M.A. White, Passive thermal management of tablet PCs using phase change materials: continuous operation, Int. J. Therm. Sci. 134 (2018) 101–115, https://doi.org/10.1016/j.ijthermalsci.2018.08.010.
[28] P.J. Shamberger, Cooling capacity figure of merit for phase change materials, J. Heat. Transfer. 138 (2015), https://doi.org/10.1115/1.4031252.
[29] L. Shao, A. Raghavan, G.H. Kim, L. Emurian, J. Rosen, M.C. Papaefthymiou, T. F. Wenisch, M.M.K. Martin, K.P. Pipe, Figure-of-merit for phase-change materials used in thermal management, Int. J. Heat. Mass Transf. 101 (2016) 764–771, https://doi.org/10.1016/j.ijheatmasstransfer.2016.05.040.
[30] P.J. Shamberger, T.S. Fisher, Cooling power and characteristic times of composite heatsinks and insulants, Int. J. Heat. Mass Transf. 117 (2018) 1205–1215, https://doi.org/10.1016/j.ijheatmasstransfer.2017.10.085.
[31] P.M. Tripathi, A. Marconnet, A New Thermal Management Figure of Merit for Phase Change Materials (PCMs) Selection Considering Geometry, in: Proceedings of the 22nd IEEE Intersociety Conference on Thermal and Thermomechanical Phenomena in Electronic Systems (ITherm), 2023, pp. 1–5, https://doi.org/10.1109/ITherm55368.2023.10177527.
[32] D.V. Ragone, Review of Battery Systems For Electrically Powered Vehicles, SAE International, Warrendale, PA, 1968, https://doi.org/10.4271/680453.
[33] K. Yazawa, P.J. Shamberger, T.S. Fisher, Ragone relations for thermal energy storage technologies, Front. Mech. Eng. 5 (2019) 29, https://doi.org/10.3389/fmech.2019.00029.
[34] R.A. Kishore, A. Mahvi, A. Singh, J. Woods, Finned-tube-integrated modular thermal storage systems for HVAC load modulation in buildings, Cell Reports Phys. Sci. 4 (2023) 101704, https://doi.org/10.1016/j.xcrp.2023.101704.
[35] F.P. Incropera, D.P. DeWitt, Fundamentals of Heat and Mass Transfer, 5th ed, J. Wiley New York, New York, 2002.
[36] K. Boomsma, D. Poulikakos, On the effective thermal conductivity of a three-dimensionally structured fluid-saturated metal foam, Int. J. Heat. Mass Transf. 44 (2001) 827–836, https://doi.org/10.1016/S0017-9310(00)00123-X.
[37] J.H. Ferziger, M. Perić, J.H. Ferziger, M. Perić, Finite Difference Methods. Computational Methods for Fluid Dynamics, Springer, Berlin, Heidelberg, 2002, pp. 39–69, https://doi.org/10.1007/978-3-642-56026-2_3.
[38] The MathWorks Inc., MATLAB version: 9.12.0 (R2022a), (2022). https://www.mathworks.com (accessed February 23, 2024).
[39] ANSYS Fluent - CFD Software | ANSYS, (2022). http://www.ansys.com/products/fluids/ansys-fluent.
[40] H.M. Ali, A. Arshad, M.M. Janjua, W. Baig, U. Sajjad, Thermal performance of LHSU for electronics under steady and transient operations modes, Int. J. Heat. Mass Transf. 127 (2018) 1223–1232, https://doi.org/10.1016/j.ijheatmasstransfer.2018.06.120.
[41] E.G. ALEXANDER, Structure-Property Relationships in Heat Pipe Wicking Materials, Ph.D, North Carolina State University, 2022 n.d, https://www.proquest.com/docview/302705989/citation/D8B43E0D35BE4122PQ/1. accessed October 28.